INFLUENCE OF PHYSICAL PROPERTIES OF VERTICAL WALL SURFACES ON HUMAN THERMAL SENSATION BASED ON FIELD MEASUREMENTS AND MICROCLIMATE SIMULATION

Kiyoshi Sasaki [1], Saori Yumino [2], Akashi Mochida [3]

[1] *Institute of Technology SHIMIZU CORPORATION, 4-17, Etchujima 3-Chome Koto-ku, Tokyo, Japan, k_sasaki@shimz.co.jp*
[2] *Tohoku University, #1206, 6-6-11, Aoba, Aramaki-Aza, Aoba-ku, Sendai, Miyagi, Japan, yumino@sabine.pln.archi.tohoku.ac.jp*
[3] *Tohoku University, #1202, 6-6-11, Aoba, Aramaki-Aza, Aoba-ku, Sendai, Miyagi, Japan, mochida@sabine.pln.archi.tohoku.ac.jp*

1. Introduction

In recent years, various countermeasures, such as greening, reflective painting, and ventilation paths, have been launched against Urban Heat Island phenomenon. One of the major purposes of these countermeasures is to create acceptable or tolerable thermal environments inside a warmed urban area. Thus, the performance of countermeasures should be assessed based on human thermal sensation as well as air temperature reduction. Previous studies have shown that radiation has a great influence on outdoor thermal sensation in summer (Mayer et al., 2008). Therefore, the physical properties of building cladding materials in relation to radiation are important factors for thermal sensation in pedestrian space. Furthermore, considering the shape of the human body, the physical properties of vertical wall surfaces have more influence on thermal sensation in pedestrian spaces than those of horizontal wall surfaces. However, the properties of building cladding materials for walls have been mainly studied for reducing the heating and cooling loads of indoor spaces. Thus, knowledge of the influence of the modification of physical properties of building cladding materials on outdoor thermal sensation must be accumulated.

In order to clarify the influence of the modification of physical properties of building cladding materials on outdoor thermal sensation, field measurements were carried out at the COSMO (Comprehensive Outdoor Scale MOdel) site, Japan, in the summer of 2011. Three types of vertical wall surfaces, i.e., concrete, greening, and high reflective material, were set up, and surface temperature, air temperature, wind velocity, and three-dimensional radiant heat transport near each wall were measured. Furthermore, the radiation and conduction simulations were conducted for the same area as the field measurements. Measured data was used to validate the simulation.

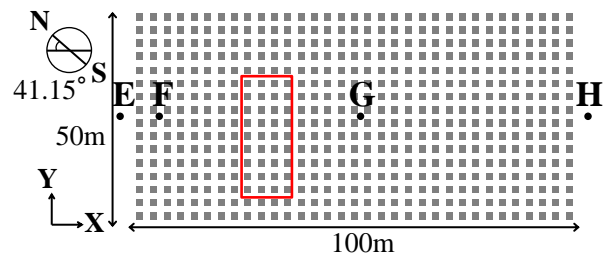## 2. Field measurements

2.1 Outline

Field measurements were carried out at the COSMO (Comprehensive Outdoor Scale Model (Inagaki and Kanda, 2008), Figs. 1 and 2) site, located within the premises of the Nippon Institute of Technology, Saitama prefecture, Japan (39°04'N, 139°07'E). Five hundred and twenty-eight 1.5 m-high concrete void cubes, with a wall thickness of 0.1 m, were arranged at COSMO site as shown in Fig. 2(1). The plan area density of the COSMO site was 0.25. The same concrete material was used for the cubes and the ground. The cubes and the ground surfaces were coated with gray diffusive paint. However, paint deterioration was often observed in 2011, particularly at the ground. The south-east surfaces of two cubes in the red rectangular zone in Fig. 2 (2) were changed to greening (GR) and high reflective material (HR), and detailed measurements around the changed surfaces were carried out

The measurement period was from August 28th to September 8th, 2011 excluding the period from August 31st to September 5th, when the measurement site was affected by a typhoon. The measured variables and measuring points are shown in Table 1 and Fig. 2, respectively.

In the interspace between two blocks, the red rectangular area written as area GR, CO and HR in Fig. 2, the three-dimensional (3D) radiant heat transport (Mayer et al., 2008; Thorsson, 2007), surface temperature, and air temperature were measured. The 3D radiant heat transport was measured at the center of each area and at point A (Fig. 3). Since the instruments were rather large compared to the measurement area, short- and long-wave radiations along the X, Y, and Z axes could not be measured simultaneously. Therefore, short- and long-wave radiations along the X and Z axes were measured simultaneously in each area, but that along the Y axis was measured at point A, as shown in Fig. 2(2), assuming the uniformity of radiant heat transport in the Y direction within the COSMO site. Surface temperatures were measured at nine points per surface, as shown in Fig. 4. Red rectangular area in Fig. 2(2) had three surfaces: the SE wall surface, NW wall surface, and ground surface, and 27 measuring points in total were set in each area. The air temperature was measured using a thermocouple at four

Fig. 1 Panoramic view of the COSMO site

(1) COSMO layout
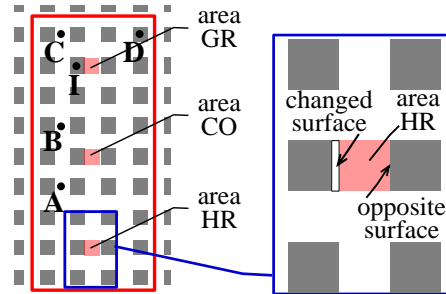
(2) Detailed plan around each vertical surface
Fig. 2 The measurement area and measuring points

Table 1 Measured variables and instruments used

site	Variables	Instruments	interval	height	Periods
Area HR	Short- and long-wave radiation (along X,Z axes)	Net radiometer	1 min	0.75 m	September 6th–7th
	Air temperature	Thermocouple(φ0.05 mm)	1 min	0.25 m 1.25 m	Entire period
	Surface temperature	Thermocouple(φ0.3 mm)	1 min	-	Entire period
Area CO	Short- and long-wave radiation (along X,Z axes)	Net radiometer	1 min	0.75 m	August 28th–30th September 6th–7th
	Air temperature	Thermocouple(φ0.05 mm)	1 min	0.25 m 1.25 m	Entire period
	Surface temperature	Thermocouple(φ0.3 mm)	1 min	-	Entire period
Area GR	Short- and long-wave radiation (along X,Z axes)	Net radiometer	1 min	0.75 m	August 28th–30th
	Air temperature	Thermocouple(φ0.05 mm)	1 min	0.25 m 1.25 m	Entire period
	Surface temperature	Thermocouple(φ0.3 mm)	1 min	-	Entire period
A	Short- and long-wave radiation (along Y axes)	Net radiometer	1 min	0.75 m	August 28th–30th September 6th–7th
B	Wind direction and wind velocity	3D Ultrasonic Anemometer	0.1 s	0.20 m 0.75 m	Entire period
C	Air temperature and humidity	Thermistor/Polymer sensor	1 min	0.75 m	August 28th–30th September 6th–8th
D	Air temperature inside block	Thermocouple(φ0.3 mm)	1 min	0.75 m	Entire period
E, G, H, F_{lower}	Air temperature and humidity	Thermistor/Polymer sensor	1 min	1.2 m	August 28th–30th September 6th–8th
F_{upper}	Air temperature and humidity	Thermistor/Polymer sensor	1 min	3 m	August 28th–30th September 6th–8th
	Wind direction and wind velocity	3D Ultrasonic Anemometer	0.1 s	3.75 m	Entire period
I	Global solar radiation	Pyranometer	1 min	1.5 m	Entire period

Fig. 3 Measurement of 3D radiant transport

(1) SE surface　　(2) NW surface
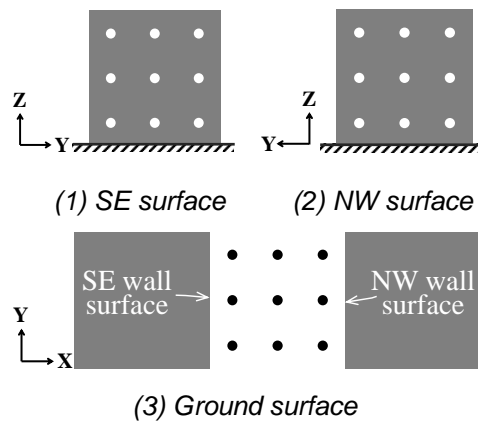

(3) Ground surface
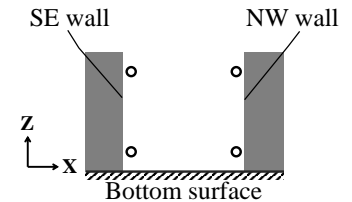
Fig. 4 Measuring points for surface temperature in red rectangular area

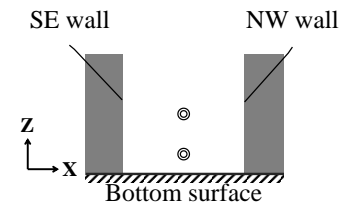Fig. 5 Measuring points for air temperature in red rectangular area

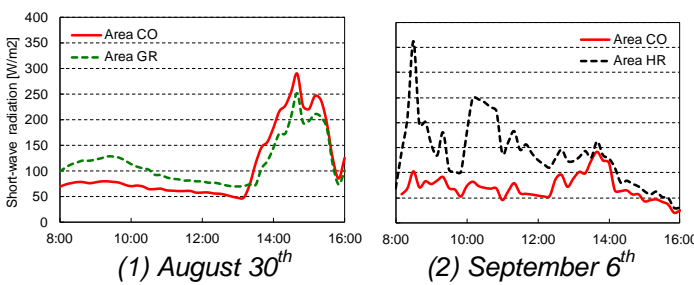Fig. 6 Measuring points for wind velocity in point B

(1) August 30th　　(2) September 6th

Fig. 7 Short-wave radiation from each changed surface
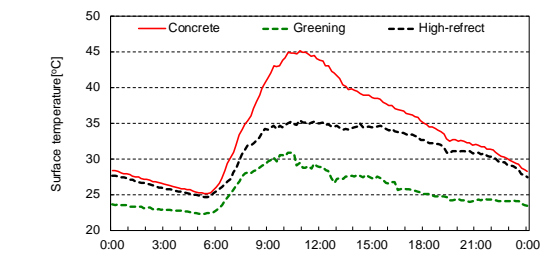
Fig.8 Surface temperature of each changed surface (August 30th)
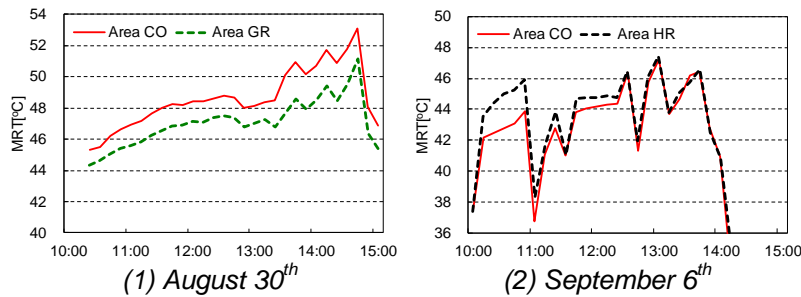

(1) August 30th　　(2) September 6th

Fig. 9 MRT at center of each area

points in each area, as shown in Fig. 5.

Furthermore, to obtain data for background conditions, global solar radiation and wind direction, wind velocity, air temperature, and humidity at the COSMO site were measured at a height of 3.75 m, at point F shown in Fig.2 (1). Inside the canopy layer of the COSMO site, wind direction, wind velocity, air temperature, and humidity were measured at representative points. Fig. 6 displays two measuring points for wind direction and wind velocity inside the canopy layer at point B shown in Fig. 2(2). In addition, air temperature and humidity were also measured outside the COSMO site at points E and H, as indicated in Fig. 2(1), to compare the thermal environment inside and outside the COSMO site.

2.2 Results

Fig. 7 shows short-wave radiation from each changed surface. From 8:00 a.m. to 1:00 p.m. when the changed surfaces were exposed to direct solar radiation, differences in the value of short-wave radiation from each changed surface became greater. During this period, short-wave radiation from the high reflective material surface was greater than that from concrete by up to about 250 W/m^2, while short-wave radiation from the greening surface was greater than that from concrete by up to about 50 W/m^2.

Surface temperatures of each changed surface on August 30th are shown in Fig. 8. The surfaces of greening and high reflective material were found almost always to be cooler than the concrete surfaces, and the difference in surface temperature between greening and concrete was up to 15°C, while that between the high reflective material and concrete was up to 10°C. However, the high reflective material surface heated up the ground and opposite surfaces more since it reflected more short-wave radiation than the concrete surface. The changes in the surface temperatures shown in Fig. 8 lead to changes in long-wave radiation from each changed surface. During the day, long-wave radiation from the greening surface was lower than that of the concrete surface by up to about 30 W/m^2, while long-wave radiation from the high reflective material surface was lower than that of the concrete surface by up to about 20 W/m^2.

MRT values were calculated from the results of 3D radiant heat transport so that the different shapes and

absorptivities of the human body in the cases of both long-wave and short-wave radiations were considered.

$$MRT = \left[\sum_{l=-3}^{3} (R_{LW}\varepsilon + R_{sw}\alpha)C_l \Big/ \sigma \right]^{1/4} - 273 \quad [°C] \tag{1}$$

where l = the index of direction of surface on cylinder (±1, 2, 3),

R_{LW} and R_{SW} = amounts of long-wave and short-wave radiations, W/m^2,

ε = long-wave absorptivity of object (in this paper, ε = 0.98 (Nakayama, 1981)),

α = short-wave absorptivity of object (in this paper, α = 0.5 (Watanabe et al., 2010), and

c_l = weight coefficient of each object surface (in this paper, $c_{\pm1}$=0.238, $c_{\pm2}$=0.238, $c_{\pm3}$=0.024 (Nakamura,1987)).

Fig. 9 compares MRT values calculated at the center of each area. The MRT at area GR was lower by up to 2.6°C than that at area CO because of the differences in the amount of long-wave radiation absorbed by the human body, caused by the differences in surface temperatures in each area (Fig. 8). However, the MRT at area HR was higher by up to 2.2°C than that at area CO because of the increase in the amount of short-wave radiation absorbed by the human body.

3. Radiation and conduction simulations

3.1 Simulation setup

Fig. 10 shows the computational domain. A set of 3 × 3 buildings were modeled, and the target area (the gray area in Fig. 10) was determined considering the uniformity of the radiant field in the COSMO site. The target date for the simulation was August 30, 2011. The unsteady analysis was performed over a period of 48 h, from 0:00 on August 29 to 24:00 on August 30. Detailed descriptions and outlines of the unsteady radiation and conduction simulation can be found in Yoshida et al. (2000a), Yoshida et al. (2000b), Chen et al. (2004), Huang et al. (2005), and Mochida et al. (2006).

Tables 2 and 3 show the calculation conditions for the unsteady radiation and conduction simulation, and the thermal properties of the cubes and the ground surface of the COSMO site, respectively.
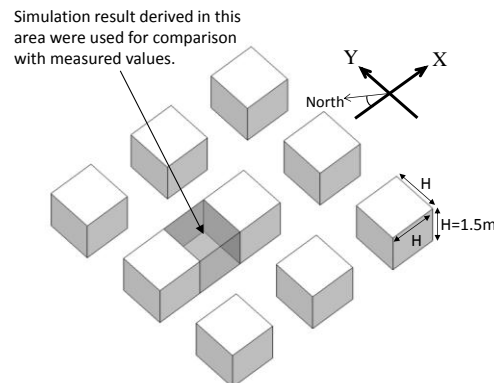

Fig. 10 The computational domain of the unsteady radiation and conduction simulation

Table 2 Calculation conditions for the unsteady radiation and conduction simulation

Calculation date (related to solar altitude)		August 30th
Calculation period		For 48 h from 0:00 a.m. on August 29th
Meteorological data		Measured values
Mesh number (x×y×z)		34×34×9
Domain size (x[m]×y[m]×z[m])		408.0×408.0×202.0
Boundary conditions	Ground	Thermal gradient was set to zero in 1.0 m of earth
	Solid surface	In: Total heat transfer coefficient, α= 9[W/m^{2}K] and interior air temperature was set to the measured value. Out: Convective heat transfer coefficient, α$_c$ = 12[W/m^{2}K] was imposed.

Table 3 Thermal properties of the cubes and the ground at the COSMO site

Materials	Ground		Concrete Cubes	Changed Surface	
	Concrete Slab	Soil		High Reflective	Greening
Thickness [mm]	150	1000	100	10	10
Albedo [-]	0.3	-	0.1	0.7	0.3
Emissivity [-]	0.9	-	0.9	0.9	0.9
Surface wetness [-]	0	-	0	0	0.7
Thermal conductivity [W/(m・K)]	1.6	2.0	1.6	1.6	1.6
Heat Capacity [kJ/(m^3・K)]	2300	3000	2300	2300	3000

At first, validation of simulation was carried out in the same situation of cubes and ground of COSMO. Next, in order to assess the thermal effects of greening and high reflective material, the cases which changed all vertical surfaces of cubes to each material were calculated.

The albedo of the concrete cubes was set to 0.1, which was the measured value, and the albedo value of the ground was set to 0.3, which was lower than the value measured at the concrete block surface. This is because the coating on the ground had been partially removed, and the color of the ground was fading.

3.2 Validation

Fig.11 shows the comparisons of calculated surface temperature values with measured values in area CO. Calculated values from the three surfaces agreed fairly well with the measured value at each surface, in terms of peak position. However, predicted values were often slightly underestimated, although the magnitude of these differences was less than 3 °C.

Fig. 12 compares the estimated radiation heat absorbed by a human body at the center of the canopy layer, with measured values. Although slight discrepancies between calculated and measured values were observed, these differences fell within 5% of the total absorbed radiation value.

3.3 Comparison of MRT and radiation heat absorbed by a human body

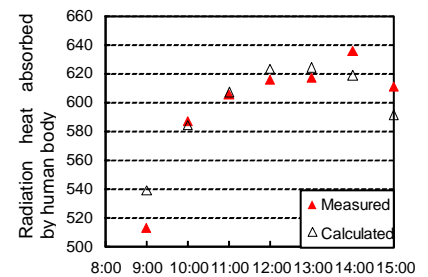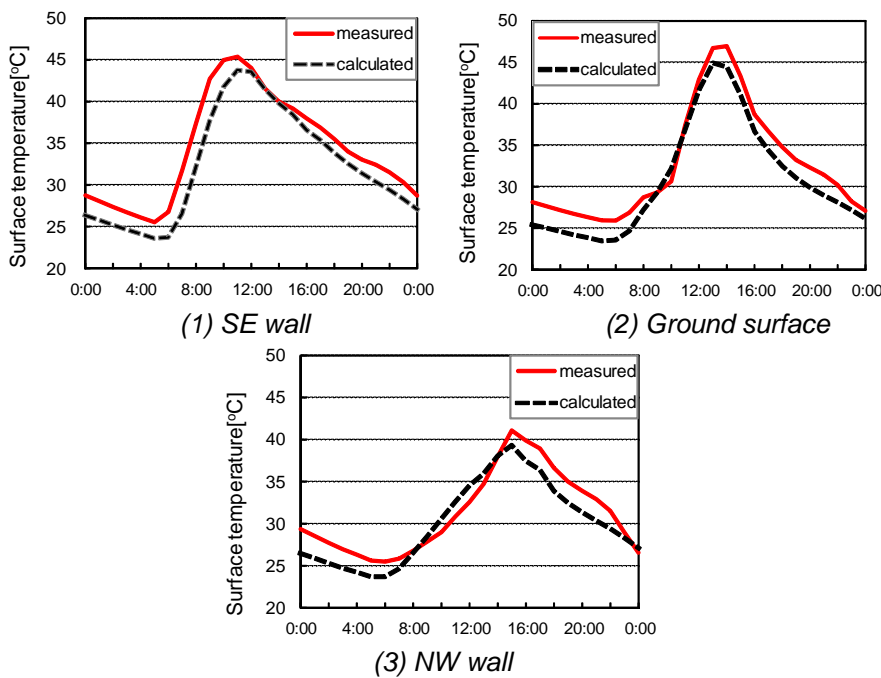Fig.13 shows the MRT difference at central plane in Y-direction between area CO and area GR, area HR

(1) SE wall

(2) Ground surface

Fig. 12 Comparisons of the
calculated radiation heat
absorbed by a human body
with measured values

(3) NW wall

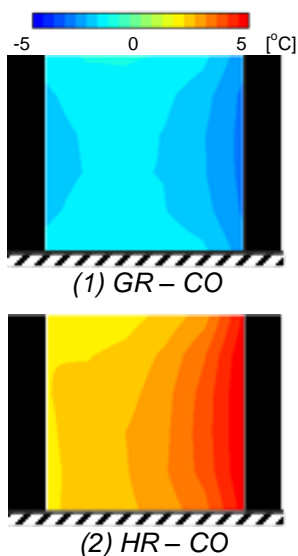Fig. 11 Comparisons of calculated surface temperatures with measured
values in area CO

(1) GR – CO

(2) HR – CO

Fig. 13 Difference of MRT
from CO

(1) GR – CO

(2) HR – CO
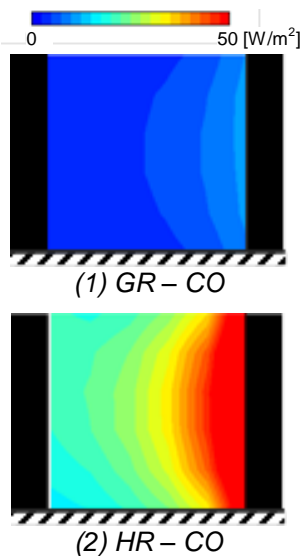
Fig. 14 Difference of short-wave
radiation heat absorbed by
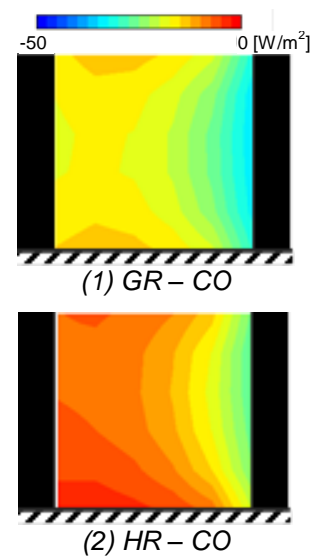a human body from CO

(1) GR – CO

(2) HR – CO

Fig. 15 Difference of long-wave
radiation heat absorbed by
a human body from CO

respectively. Additionally, differences of short-wave and long-wave radiation heat absorbed by a human body at the same plane as MRT difference are shown in Figs.14 and 15. The MRT value at area GR was lower on an average of 1.9 °C than at area CO because of the much reduction in the amount of long-wave radiation absorbed by the human body (Fig.15(1)). The amount of long-wave radiation absorbed by the human body at area HR was lower than at area CO (Fig.15(2)), but the amount of short-wave radiation absorbed by the human body at area HR was much higher than at area CO (Fig.14(2)). As a result, the MRT value at area HR was higher on an average of 2.7 °C than area CO.

4. Conclusion

Field measurements were carried out near the three types of vertical walls and the radiation and conduction simulations were conducted for the same area. Calculated values of surface temperature agreed fairly well with the measured value in terms of peak position. The estimated absorbed radiation by a human body at the center of the canopy layer was compared. Although slight discrepancies between calculated and measured values were observed, these differences fell within 5% of the total absorbed radiation value.

The surfaces made of greening and high reflective material were found to almost always be cooler than the concrete surface, but the high reflective surface heated the ground and wall surfaces of neighboring buildings more than the others since it reflected more short-wave radiation. It was estimated that a human body standing near the high reflective surface would absorb the radiant heat more than when standing near the concrete, and among the three cases compared here, the radiant environment was evaluated to be the worst for the high reflective surface.

Acknowledgment

References

Chen, H., Ooka, R., Harayama, K., Kato, S., Li, X. (2004): Study on outdoor thermal environment of apartment block in Shenzhen, China with coupled simulation of convection, radiation and conduction, *Energy and buildings*, **36**, 1247-1258.

Huang, H., Ooka, R., Kato, S. (2005): Urban thermal environment measurements and numerical simulation for an actual complex urban area covering a large district heating and cooling system in summer, *Atmospheric Environment*, **39(34)**, 6362-6375

Inagaki, A. and Kanda, M. (2008): Turbulent flow similarity over an array of cubes in near-neutrally stratified atmospheric flow, *Journal of Fluid Mechanics*, **615**, 101-120

Mayer H., Holst J., Dostal P., Imbery F., and Schindler D, 2008: Human thermal comfort in summer within an urban street canyon in central Europe, *Meteorol. Zeitschrift*, **17**, 241-250

Mochida, A., Yoshino, H., Miyauchi, S., Mitamura, T., (2006): Total analysis of cooling effects of cross-ventilation affected by microclimate around a building, *Solar Energy*, **80**, 371-382.

Nakamura Y., (1987): Expression Method of the Radiant Field on a Human Body in Buildings and Urban Spaces, *Journal of Architecture, Planning and Environmental Engineering*, **376**, 29-35 (in Japanese)

Nakayama A., (1981): Thermophysiology, *Rikogakusha Publishing Co., Ltd*, Japan

Thorsson S., Lindberg F., Eliasson I. and Holmer B., (2007): Different methods for estimating the mean radiant temperature in an outdoor urban setting, *International Journal of Climatology*, **27**, 1983-1993

Watanabe S., Horikoshi T. and Tomita A., (2010): Measurement of solar radiation absorptance of clothed human body in outdoor, *Japanese Journal of Biometeorology*, **47**, 165-173 (in Japanese)

Yoshida, S., Murakami, S., Ooka, R., Mochida, A., Tominaga, Y. (2000a): CFD prediction of thermal comfort in microscale wind climate, *Proceedings of the 3rd International Symposium on Computational Wind Engineering*, 27-30.

Yoshida, S., Murakami, S., Mochida, A., Ooka, R., Tominaga, Y., Kim, S. (2000b): INFLUENCE OF GREEN AREA RATIO ON OUTDOOR THERMAL ENVIRONMENT WITH COUPLED SIMULATION OF CONVECTION, RADIATION, AND MOISUTURE TRANSPORT, *Journal of Architectural Planning Environment and Engineering*, **529**, 77-84 (in Japanese)